RSC Advances

ROYAL SOCIETY OF CHEMISTRY

www.rsc.org/advances

A novel synthesis of Fe_2O_3@activated carbon composites and its exploitation for the elimination of carcinogenic textile dye from aqueous phase

Ruhul Amin Reza, M. Ahmaruzzaman*
Department of Chemistry, National Institute of Technology Silchar, 788010, India

A B S T R A C T: The present work reports the synthesis of Fe_2O_3@activated carbon composites by co-precipitation of iron salts onto activated carbon. The prepared composite was explored for remediation of a carcinogenic textile dye, Remazol Brilliant Blue R (RBBR) from aqueous solution. The surface morphology, composition and textural characteristic of the prepared magnetic composite (FAC) were investigated by FTIR, SEM-EDS, XRD, TEM, Selected area electron diffraction (SAED), VSM, TGA, surface area, and pore size. TEM images showed that the prepared composites were wire shaped. The saturation magnetization value (26.99 emu/g) was sufficient for magnetic separation in wastewater treatment. Owing to the unique micro-mesoporus structure, high surface area (1199 m^2/g), and pore volume make (0.9909 cm^3/g) further enhances its utilization for the treatment of dye laden wastewater. The pseudo-second-order kinetic model with high correlation coefficients (R^2> 0.999) was suitable to describe the process of RBBR adsorption onto FAC. The Langmuir model fitted the adsorption isotherm data better than the Freundlich, Temkin and DR model. Values of thermodynamic parameters (ΔG°, ΔH° and ΔS°) indicated that the adsorption process was strongly dependent on temperature of the aqueous phase, and spontaneous and exothermic in nature. Therefore, FAC composite displays main advantages of excellent dispersion, convenience separation and high adsorption capacity, which implies their potential application in the environmental cleanup process.

Keywords: *Composite material, magnetic, Adsorption, RBBR, Ionic strength*

Corresponding author (M. Ahmaruzzaman; md_a2002@rediffmail.com)

Introduction

The rapid industrialization, urbanization, and unplanned activities of human being significantly enhanced the environmental pollution. Every year world-wide about 50,000 tons of dyes are discharged into the environment [1] causing a serious environmental impact in the ecosystem. Nowadays government legislation is becoming stricter regarding the removal of carcinogenic, toxic dyes from industrial effluents, especially in the more developed countries [2]. The industrial effluents are toxic and characterized by high biological oxygen demands (BODs), chemical oxygen demands (CODs), suspended solids and intense color [3]. Dyes producing and consuming industries, such as food, paint, plastic, cosmetics, printing and pharmaceutical industries generate a huge volume of toxic wastewater contaminated with coloured synthetic dyes [4]. These dyes in aquatic system interferes photosynthesis of aquatic plants/life, hinders the growth of microbes, moreover, the mutagenic and carcinogenic nature of dyes is threat to the human health [5]. Due to synthetic origin and aromatic nature, dyes are biologically non-degradable and hence it is rather difficult to treat dye containing wastewater [6]. Remazol Brilliant Blue R dye (RBBR) is one of the most important dyes in the textile industry. It is frequently used as a starting material in the production of polymeric dyes. It is an anthracene derivative and represents an important class of toxic and recalcitrant organo pollutants.

Activated carbon (AC) is a most widely used versatile adsorbent material for various for the removal of organic and inorganic contaminants from wastewater. However, AC is difficult to retrieve, separate, and regenerate when it is exhausted. The traditional method for separating the powdered AC could cause the blockage of filters and loss of AC. The traditionally discarded process sludge process of the spent adsorbent, resulting in the secondary pollution [10,11]. The difficulties of powder AC is overcome by magnetic AC composite, an effective and low-cost

adsorbent, has attracted a lot of attention nowadays. The functional nanoporous materials nowadays have widely used as efficient adsorbents for environmental cleaning purpose [12-14]. Recently magnetic filtration is emerging technology in wastewater treatment process which can provide rapid, efficient contaminant removal from aqueous waste streams [15]. Inexpensive adsorbents could be developed that can bind to environmental contaminants and then be magnetically separated. The advantages of magnetic activated carbon adsorbents over the traditional adsorbents are that it can easily be separated from solution using a magnetic separator even if the solution contains a significant concentration of solids.

The present work addresses the development of eco-friendly, low cost activated carbon from a biomass source and further magnetized by co-precipitation of iron salts onto activated carbon for the treatment of simulated reactive dye effluent (RBBR). Iron oxide/activated carbon magnetic composite were characterized by FTIR, SEM-EDX, TEM, P-XRD, VSM, surface area and pore size. The adsorption behavior of the composite materials was performed in batch mode, studying the impact of operational parameters (pH, adsorbent dose, temperature, and interaction time). The experiments are also carried out to observe the impact of ionic strength, salt, and hardness on the removal of RBBR from aqueous phase. Simulated mixture is also prepared to see the effect on the removal of RBBR. The adsorption process was carried out in batch system with emphasis on kinetics, isotherm modeling and error analysis.

Materials and methods

Materials

The dye used as target molecule for the adsorption evaluation of magnetic carbon was Remazol Brilliant Blue R (Acronym: RBBR; MF: $C_{22}H_{16}N_2Na_2O_{11}S_3$; MW: 626.54 g/mol; λ_{max} = 595 nm; purity = 99%) are procured from Sigma-Aldrich. All chemicals were purchased from

Merck (India) in analytical purity and used in the experiments directly without further purification. All the solutions were prepared using ultrapure water from Mili pore water purification system (Model: ELIX 3S KIT (IL), France).

Development of activated carbon and synthesis of Fe_2O_3@activated carbon composites

The precursor, *Schumannianthus dichotomus*(SD) obtained from nearby village. It was dried in the oven at 383K for 24 h and saturated with sufficient amount of concentrated ortho-phosphoric acid. The impregnation time was kept for 1 h to obtain uniform mixture. Then acid impregnated SD was carbonized at 773 K in the muffle furnace (Alfa Instruments) for 1 h at a constant heating rate of 283 $K.min^{-1}$ under an inert atmosphere. The carbonized materials was washed with pure water, dried, grounded and stored in the dessicator until use.

The impregnation of AC with hematite was achieved by co-precipitation of the two salts of iron ($FeCl_3$ and $FeSO_4$) on activated carbon. A freshly prepared $FeCl_3$ (3.46 g in 250 ml) $FeSO_4$ (13.3 g in 100 ml) solution is mixed and vigorously stirred at 333 K for 30 min. The mixed solution of iron salts was added successively into the aqueous suspension of activated carbon at 303K prepared in the earlier stage and stirred in magnetic stirrer for 40 mins. The resulting solution was precipitated by adding drop wise 2M NaOH solution with continuously vigorous stirring. During the reaction process, the pH was maintained at about 10-11. The suspension was further mixed for 1 h and aged at room temperature for 24 h. The suspension was repeatedly washed with distilled water followed by ethanol and then finally dried in the vacuum oven at 353K. The developed adsorbent is known as magnetic activated *Schumannianthus dichotomus* (FAC).

Analytical techniques for Characterization

Spectroscopic characterization (FTIR, SEM-EDX, XRD, TEM, SAED)

Fourier Transform Infrared (FT-IR) Spectroscopic analysis of the adsorbent sample was performed on a Nicolet MAGNA-550 FTIR Spectrophotometer in the range 400-4000 cm^{-1} to characterize the functional groups on the surface of the adsorbent.

The texture and morphology of the adsorbent was examined by a Scanning Electron Microscope ((FEG-SEM, Model: JSM-7600F, Magnification: x25 to 1,000,000)). The sample was first gold coated using Sputter Coater, Edwards S150, which provides conductivity to the sample, and then the SEM micrograph were taken.

The Powder X-ray diffraction (XRD) patterns were studied on a X-ray Diffracto-meter (Model: Philips X'pert MPD system) with X'pert software using 30 mA, 40 kV, Cu K radiation (k = 1.546 Å). JCPDS database and indexed with POWD software for qualitative analysis of the orientation of plane of the adsorbents. The interlayer spacing ($d_{h\ k\ l}$) is determined using the Bragg's equation given as:

$$d = \frac{\lambda}{2\ \mathrm{Sin}\,\theta} \quad (1)$$

where λ is the wavelength of X-ray used and θ is the scattering angle. The crystallite size is determined from the half width of the diffraction peak using the Scherrer equation:

$$L = \frac{K\,\lambda}{B\ \mathrm{Cos}\,\theta} \quad (2)$$

where L is average crystallite size, B is the full width half maxima of the peak, and K is the shape factor.

The TEM images and SAED pattern of magnetic and non magnetic activated carbons were recorded using PHILIPS, CM200 Transmission Electron Microscope operated at an

accelerating voltage: 20-200 kV Resolution: 2.4 Aº. Samples were deposited onto carbon coated grid, and surface morphology is studied.

Textural characterization of the carbon samples (Surface area, pore size)

Micromeritics, ASAP 2010 Surface Area Analyzer was used to determine the textural features of the adsorbent. N_2 adsorption/desorption isotherm at 77.71 K in the relative pressure (P/P0) range was used to determine the Brunauer–Emmett–Teller (BET) surface area by using the Brunauer et al. Equation . BJH (Barret–Joyner–Halenda) desorption method was used to compute the cumulative volume and average pore diameter of the pores. The particle size analysis of the adsorbent was done on a Malvern Mastersizer 2000 Particle Size Analyser.

Hysteresis and magnetic moment measurements

The magnetic properties of a ferromagnetic material are represented by plots of magnetization (M) against the field strengths giving the hysteresis loop. The hysteresis measurements were carried out on Lakeshore VSM 7410 Susceptometer at room temperature (300K) in a magnetic field that varied from -15000 Oe to +15000 Oe.

Experimental procedure and data analysis

The retention of RBBR in batch system was carried out in a series of 100 mL stopper Erlenmeyer flasks to examine the effects of influencing parameters viz. initial pH (pHo), interaction time (t), adsorbent load (m), and temperature (T). The experiments were conducted in a temperature controlled incubator cum shaker (shaking speed: 180 rpm) at various temperatures (303, 313, 323) K. At the end of pre-determined time the samples were withdrawn, (centrifuged at 5000 rpm for 2 min) and the supernatant was analyzed for the residual concentration of RBBR.

The residual concentration in the supernatant solution was determined using an UV–Visible Spectrophotometer (Thermo Scientific) at λ_{max} = 595 nm. The percentage removal and adsorptive uptake of RBBR were estimated using the following mass-balance equations:

Percentage removal of RBBR: $q_e = \frac{(C_o - C_e)100}{m}$ (3)

Adsorptive uptake of RBBR per g of adsorbent: $q_m = \frac{(C_o - C_e)V}{m}$ (4)

where C_0 = initial RBBR concentration (mg L^{-1}), C_e = equilibrium RBBR concentration (mg L^{-1}), V is the volume (L) of RBBR sample taken, and m is the weight (g) of the adsorbent.

Result and Discussions

Interpretation of characterization analysis

FTIR spectroscopy

The functional groups of FAC can be better understood from a FTIR (Fourier Transform Infra-red) study of the adsorbent. The spectra can therefore help in interpretation of the functional groups accountable for adsorption. The FTIR spectra of the AC and FAC are given in Fig1. The AC displays absorption bands at 3420, 2380, 1725 and 1180 cm^{-1}. The FTIR spectrum of AC depicts a relatively broad peak at 3420 cm^{-1} which is due to H-bonded OH stretch confirming the presence of hydroxyl group. The position and shape of the band at 3420 cm^{-1} are compatible with the involvement of hydrogen bonded hydroxyl groups. The OH groups of alcohol, phenol and carboxylic acid are located at 3625 cm^{-1}, 3605 cm^{-1} and 3530 cm^{-1}, respectively. The self-associated OH groups centered at 3400 cm^{-1} predominate in AC. The band at 3420 cm^{-1} is slightly broader towards lower wavelengths suggesting that some OH-ether

hydrogen bonds are present. The appearance of weak bands at 1300–1000 cm^{-1} indicate the presence of both hydroxyl and ether type C–O structures in AC.

FAC exhibits peak at 3411, 1580, and 936 cm^{-1} and two additional, overlapped bands at 692 and 587 cm^{-1}, compatible with the presence of iron oxides in the prepared composite. These bands were situated very close in frequency for iron oxide (γ-Fe_2O_3) in the carbon matrix [16].

Energy dispersive X-ray spectroscopy

The SEM/EDX analysis spectra of AC, before and after magnetization are shown in figure (Fig.2 (a), 2(b)). The elemental composition of AC is carbon, oxygen, nitrogen and no peak for iron was observed. Fig. 2(b) confirms the presence of Fe, O and C on the FAC surfaces. The spectra shows that the atomic percentage of oxygen of FAC is increased (10.63 to 24.73) % indicating the formation of iron oxide on the surface. The appearance of additional peaks for phosphorous probably because of the activating agent, H_3PO_4.

Transmission electron microscopy and SAED pattern

The Transmission Electron Micrographs of FAC are shown in the Fig.3 (a-d) and morphology is found to be different from AC. The prepared FAC was observed to be wire shaped with typical diameter in the range of ~ 57.07 to 218.36 nm. The Fe_2O_3 interacts with the surface of the AC by chemical linking [17]. This may lead to the change in surface morphology of FAC. However, further study is required to know more about any changes in morphology. The individual properties of metal oxide have been modified by encapsulating them in carbon material like activated carbon [18]. The appearance of diffraction rings and bright spots represent the higher degree of crystallinity of the particles as shown in the SAED pattern of FAC (Fig. 3(c-d)). The spots of FAC before magnetization could be indexed as (1 2 0), (0 0 2) and (1 1 0). The additional spots in Fig. 3(d) could be indexed corresponding to the

reflections from the (0 1 2), (1 1 0), (2 0 2), (0 2 4), (0 1 8), (3 0 0), (2 1 4) lattice plane and matches well with the JCPDS values (89-2810) of hematite, iron oxide in the pores of carbon matrix**.**

Crystalline properties (P-XRD)

The powder XRD pattern of AC before mangnetization **(**Fig.4a**)** portrays broad diffraction peaks at around 2θ values of 14.86, 22.94 and 26.47 which can be ascribed to the hexagonal carbon like reflections (JCPDS file No. 50-0926). The stack of parallel layers results in the highest intensity peak at 2θ = 26º signifying the existence of graphitic ordering in the molecular planes and the interlayer spacing $d_{(1\ 0\ 3)}$ = 0.336 nm is calculated with the help of Eq. (1). It needs to be mentioned that the d value is greater than that of graphite (0.335 nm) confirms the disordered framework far from graphitization. The average crystallite size computed from the Scherrer equation is 11.18 nm.

Hematite impregnation of activated carbon showed iron content of 26.58% in magnetic sample. The co-precipitated iron component was examined by the X-ray diffraction patterns. The X-ray diffraction pattern for FAC (Fig.4b) displayed a number prominent Bragg reflections which are compatible with the presence of $Fe(OH)_2$ and $Fe(OH)_3$ (peaks at 2θ = 36.63, 38.85, 39.48 and 60.746◦) and of Fe_2O_3 (peaks at 2θ = 49.437, 53.64 and 63.43). The diffraction peak at 2-theta values of 24.2, 33.2, 35.7, 40.9, 49.5, 54.1, 63.3 and relative intensity are reasonably close to the standard data for rhombohedral centered Hematite, iron oxide lattice (JCPD file No. 89-2810). From Fig. 4(b) the appearance of five peaks are indexed as (1 1 0), (0 0 6), (1 1 3), (1 1 6), and (3 0 0). The presence of these peaks matched well with the JCPDS value (89-2810) of Fe_2O_3 corroborating the presence of iron oxide nano particles in the pores of carbon.

These iron oxides may form via the following tentative reaction paths. The solubility product constant for Fe $(OH)_3$ ($=10^{-36}$) is higher than that of $Fe(OH)_2$(10^{-14} to 10^{-17}). Initially, as the pH increases, $Fe(OH)_3$ will be precipitated during the magnetization of AC.

Step –I: Ferrous hydroxide may be oxidized by dissolved oxygen

$2Fe(OH)_2 + 1/2O_2 + H_2O \rightarrow 2Fe(OH)_3$

Step-II: During oven-drying by air:

$2Fe(OH)_2 + 1/2\ O_2 \rightarrow Fe_2O_3 + 2H_2O$

Hysteresis and magnetic moment measurement

The suitability of magnetic material for application depends on the characteristics shown by their hysteresis loops [19], obtained from plots of magnetization (M) against the field strengths. Magnetization properties were investigated at 300 K by vibrating sample magnetometer (VSM) which quantified the magnetic behavior. FAC was exhibited paramagnetic behavior, characterized by strong magnetic susceptibility. The saturation magnetization value of FAC found to be 26.99 emu/g, which is strong enough for the convenient magnetic separation. The coercivity and retentively of FAC determined from VSM data are 0.303 G and 2.305 emu/g, respectively. The carbon sample without iron impregnation does not show any magnetic properties at 300 K (Fig.5).

Textural characteristics

The porous and higher surface area are important features of a good adsorbent for wastewater treatment. The RBBR dye molecules can easily adhere onto the surface of FAC as the BET surface area was found to be 1199.98 m^2/g. The single point surface area 1164.87 m^2/g was almost comparable to the BET surface area. According to IUPAC classification, N_2

adsorption/ desorption isotherm plot of FAC belongs to type –II. Pore structure and pore volume are important factors for efficient adsorption of dyes. If the pore diameter of adsorbent is lesser than the pore diameter of adsorbate molecules, then lesser adsorption would take place due to steric hindrance. The pore distribution size distribution of the FAC computed either BJH method is shown in Fig.6. FAC shows very narrow pore size distribution. The pore opened at the both end is found to be nil. At a relatively low pressure of N_2 adsorption-desorption isotherm, hysteresis loop was observed. The pore distribution shows that pores are in diameters range of 1-18 nm with average diameters of 4.2 nm. The targeted dye, RBBR having diameter of 2.1 nm can easily penetrate into the pore of the FAC [20]. According to the IUPAC classification of pore dimensions, there are three broad classifications grouped as micropore (diameter, $d \leq 2$ nm), mesopore ($2<d<50$ nm) and macropore ($d \geq 50$ nm)[21]. Maximum pore are mesopores followed by a small fraction of micropores. The total pore volume (single point adsorption) of MSD is 0.9909 cm^3/g and can verily accommodate the dye molecules. The investigation on pore volume and surface area revealed that the prepared composite may be suitable for the adsorption of RBBR molecules from wastewater.

Thermo Gravimetric Analysis

The thermal degradation characteristics of pre and post activated adsorbent are determined by thermo gravimetric analysis. The TGA curves (Fig.7) of AC, before and after activation exhibited two main weight loss regions. The weight loss (up to 70%) region from (250-350) °C shifted to (500- 600) °C after activation. Hence the activation leads to an increasing stability of the prepared adsorbent. After activation, a small weight loss was observed below 100°C, and can be attributed to the dehydration and elimination of oxygen-containing functional groups from the surface. The second rapid weight loss region after activation may be

attributed to the decomposition of organic matter. The maximum degradation temperature after activation increases from 500 °C to 700 °C. This indicates that the stability of the prepared adsorbent increased after activation by phosphoric acid.

Optimization of operational parameters (pH, adsorbent load, interaction time and temperature)

The zeta potential of the adsorbent, degree of ionization, and solubility of the adsorbate are remarkably affected by the pH of the medium. The adsorption system usually depends on the degree of speciation of adsorbate and the dissociation of functional group of the adsorbent which varies accordingly at different pH values [22]. The percentage removal of RBBR was studied as a function of pH (3–9). The maximum removal percentage of 99% for RBBR was observed at pH of 3-4. In aqueous solution, the reactive dye molecule dissolved and converted into their corresponding dye anions, DSO_3^- and Na^+. These dissociated dye anions were migrated from solution to the surface of the FAC and adsorption occurs through the electrostatic attraction. When the pH was increased (4–9), the electrostatic interaction between the dye anion and composite becomes repulsive and also, the competition between OH^- ion and the reactive dye anions had reduced the adsorption rate of dyes onto FAC. This was confirmed by the pHpzc value (6.8) of the FAC composite. Generally, the adsorption of dye anions is highly favored at pH < pHpzc[23]. Thus, limited adsorption of RBBR was observed in neutral and alkaline pH, and it could be due to the combination of other factors, such as van der Waal's forces and hydrogen bonding.

The experiments are performed to optimize the load by agitating 25 ml of RBBR solution (100 mg/L) with varying adsorbent. The uptake of RBBR remarkably enhances up to 0.8 g/L and

thereafter, a pleatu has reached. The removal efficiency has remained unaffected for the further increases in the adsorbent load. At the initial stage, the high concentration of RBBR in the bulk solution increases the adsorbing tendency of RBBR molecules in the unoccupied active site of the FAC. On the contrary, at the later stage the efficiency of the adsorbent shows marginal increment due to the overcrowding of the particles. This stage indicates the attainment of the equilibrium of RBBR molecules at the surface of FAC**.** A comparison of % removal of FAC with AC showed that there is no significant increase in the adsorption efficiency of FAC (Fig. 8). However, the presence of Fe_2O_3 in the composite indicates mainly the magnetic separation of dyes from the aqueous phase and activated carbon is responsible for the adsorption [24, 25]. They can be easily recovered by external magnetic field and can be reused again.

The experiments were performed to evaluate the interaction time for the uptake of RBBR onto the FAC. The removal of 94.82% was achieved in the initial 10 min of interaction time followed by slow increment of adsorption with lapse of time up to 60 min. A saturation condition was achieved thereafter which is indicated by pleatu line to a maximum contact time of 120 min. The high concentration gradient of RBBR solution onto the surface of the FAC aids a bulk transport of RBBR molecules from the liquid phase into the solid surface of the adsorbent. We have been observed that after 80 min of interaction time the rate of increment is negligible. Hence it can conclude that the quasi-equilibrium state was reached at the interaction time of 60 min. Therefore, the optimum interaction time of 60 min was chosen to execute the subsequent adsorption experiments.

The solution temperature is one of the key parameters to impact in the rate of adsorption. The experiments were executed under the reaction condition varied from 303K to 323K and portrayed that the adsorption capacity of RBBR onto FAC decreased with increase in

temperature (Fig. 9). This may due to the fact that entropy of the RBBR molecules increases in the surface that leads to movement of adsorbate from solid surface to liquid solution phase. On the basis of adsorption capacity, the optimum reaction temperature was kept at 303K to perform other experiments.

Impact of water characteristics (Ca^{2+}, Mg^{2+}, SO_4^{2-}, Cl^-, SDS etc.) on removal of RBBR

The adsorption capacity of FAC for RBBR in the presence of Ca and Mg was compared by performing the blank experiment. The result suggested that the presence of hardness producing salts, such as Ca and Mg has little effect on adsorption of RBBR (Fig. 10). The percentage removal is decreased from 99% to 97%. The decrease in efficiency can be attributed to the competitions of Ca and Mg for occupying the active site of the adsorbent that leads to earlier saturation of the surface in the simultaneous presence of these divalent ions.

The real dye industry wastewater contains different concentration of salts apart from the target dyes. Therefore, it is very important to investigate the impact of chlorides, sulphates, and surfactant on the adsorption of RBBR. The influences on adsorption were studied by varying the concentration (0 to 70 mM) and the results were presented in Fig. 11. The study reveals that the presence of these salts has impact on the adsorption of RBBR onto FAC. The percentage removal was reduced with increase in concentration of anions. The impact on the removal efficiency was maximum in the case of surfactant and followed the order: surfactant> sulphate> salt> chloride. The removal percentage was reduced to 93.56, 95.3%, 94.49% and 97.36%, for surfactant, sulphate salt and chlorides, respectively, whereas almost 99% removal was achieved in the absence of these anions. The decline in the efficacy of adsorbent may be due to fact that the active site of the adsorbent was blocked by these anions. The electrostatic repulsion may also play a role in decreasing the adsorption capacity of the prepared composite.

A simulated mixture was prepared by adding chlorides, sulphates, nitrate, Sodium, potassium, calcium, and magnesium. Adsorption test was performed to observe the impact on the removal of RBBR by FAC. The presence of various ions along with target dye reduced the percentage of adsorption to 96 % (Fig. 12). The reason can be attributed by the fact that the relative competition among the ions (Ca^{2+}, Na^{+}, NO_3^{-}, Cl^{-1}, K^{+}, and Mg^{2+}) species for the active sites of FAC plays an important role in decreasing the rate of adsorption. The increased numbers of cations /anions render the surface of FAC not easily accessible for dye molecules, and hence decreasing the rate of adsorption. When solid adsorbent is in contact with adsorbate molecules in solution, an electrical diffused double layer is surrounded the adsorbent/adsorabe species and thickness of the layer is significantly expanded by the presence of electrolytes. Such expansion forbids the approaching of the dye molecules towards the adsorbent surface [26].

Thermodynamics feasibility study for removal of RBBR

The computed thermodynamics parameters revealed that the negative value of standard enthalpy ($\Delta H°$ = -13.68 kJ/mol) confirming the exothermic nature of adsorption process. The negative value of entropy change ($\Delta S°$ = -2.18 J/mol K) signifies the decrease in randomness of the adsorption system at the liquid/solid interface. The decrease in Gibbs free energy value (ΔG; -13.01 to -12.97) kJ/mol with increase in temperature signifies the feasibility and spontaneity of the adsorption process. The free energy ranges of chemisorptions and physisorption are (-20 to 0) kJ/mol and (-80 to – 400) kJ/mol, respectively [27]. The reported free energy change indicates that adsorption of RBBR onto FAC is physiosorption in nature.

Adsorption Isotherm and kinetic assays

The experimental adsorption data for RBBR removal at different time interval was examined with four kinetic models viz. Pseudo first order, pseudo second order, Elovich equation and liquid film diffusion [28]. The result indicates that the rate of adsorption is very fast and reaches equilibrium within 1 h. The relatively high kinetics reflect good congregation of RBBR molecules in the binding sites of FAC. The pseudo-second order kinetic model shows very high regression coefficient (<0.99) over the other investigated models (Table 1). The experimental q_e value for pseudo second order kinetic model is agreed well with the calculated values. The least standard deviation value also justified the validity of pseudo second order over the other models. The data of different kinetic models were compared with the experimental kinetic data as shown in Fig. 13. It has been observed that pseudo second order model is fully superimposed with the experimental data. The other models shows highly scattered values from the experimental observation, which further validated that the rate of adsorption was mainly governed by pseudo second order kinetic model.

Batch mode executed experimental data were fitted to Langmuir, Freundlich and Temkin and DR isotherms mode[29, 30] to obtained the best isotherm model. The experimental data well explained by Langmuir model (Fig. 13**)** for the target dye molecules having linear regression coefficient of 0.9513~0.9871 at all studied temperatures (303~ 323 K) (Table 2). A comparison of the experimental adsorption data with the linearized plot of Freundlich, Langmuir, Temkin and Dubunin Radushkevich models is shown in Fig. 14. A high scattering from experimental values were observed in case of Temkin and Dubunin Radushkevich, while Langmuir isotherm curve was almost superimposed by experimental data followed by Freundlich. On the basis of highest correlation, low error function values and comparison of data, the fitting of different

models followed the order: Langmuir> Freundlich> Temkin> Dubunin Radushkevich. The theoretical monolayer adsorption capacity computed was found to be 211.05 $mg.g^{-1}$.

Mechanism of adsorption

The proposition of mechanism in the adsorption study is still the foremost challenge. Various factors that play important role in the establishment of adsorption are the structure of adsorbate and functional groups, textural and surface chemistry of adsorbents, and the specific interaction between adsorbent surface and adsorbate [31]. It seems that that the mechanism of interactions between carbonaceous materials and adsorbate is the π–π stacking: the carbon surface of the adsorbent interacts with the π-electron of aromatic ring of the adsorbate (RBBR). The similar type of mechanism is also reported in the literature [31, 32]. Adsorption onto the magnetic material attached on the carbon surface also taken place via π–π stacking [33]. The band at 1050 cm^{-1} in FTIR spectra can be attributed to phenols or to the formation of hydroxyl species (–FeOH/Fe–OH–Fe). The band indicate that hydroxyl species may be additionally get involved in binding of the dye molecules on the surface of carbon matrix. The proposed mechanism is shown in Fig.15. However, further study is required to establish the mechanism of RBBR dye molecules onto the surface of the prepared composite.

Concluding notes

This work demonstrated the development of paramagnetic adsorbent from the waste biomass via precipitating the mixture of Fe^{2+} and Fe^{3+} salts by NaOH solution and its application in the removal of carcinogenic textile dye, RBBR. The TEM micrographs of the prepared adsorbent confirmed the presence of magnetite wire shaped composite with average typical diameter of 57.07 ~218.36 nm. The P-XRD studies confirmed the formation of hematite iron oxide on the surface of carbon matrix. The Freundlich and Langmuir isotherm fitted the

experimental data well. The adsorption of RBBR onto FAC followed pseudo second-order equation. The 99% MB were absorbed in 10-20 min, and the pseudo second order kinetic model was feasible to describe the RBBR adsorption process in Fe_2O_3/activated carbon composite. The prepared composite showed both good magnetic response and high BET surface area (1099.98 $m^2\ g^{-1}$). The FAC composite could be easily separated and retrieved by an outer magnet after the removal of contaminants from water. This prepared carbon composite is easily re-dispersed into the solution after removing the magnetic field. Therefore, from practical point of view, the prepared AC/Fe_2O_3 composite material would be promising magnetic adsorbent for the removal of dye from wastewater.

Acknowledgement

The authors are thankful to Director NIT Silchar, for providing laboratory facility and financial assistance for analysis of the developed adsorbents. One of the authors is thankful to the University Grant Commission (UGC), New Delhi for financial assistance under Maulana Azad National Junior Research Fellowship (MANJRF) in completion of the research work.

Literature cited

[1] Osama, J. F; Toca-Herrera, J. L; Rodriguez-Couto, S. Transformation pathway of Remazol Brilliant Blue R by immobilised laccase. Bioresource Technology 2010, 101, 8509-8514.

[2] O'Neill, C.; Hawkes, F.R.; Hawkes, D.L.; Lourenco, N.D.; Pinheiro, H.M.; Delee, W. Colour in textile effluents-sources, measurement, discharge consents and simulation: a review. J. Chem. Technol. Biotechnol. 1999, 74, 1009-1018.

[3] H. Zollinger, Colour Chemistry—Syntheses, Properties and Application of Organic Dyes and Pigments, VCH Publishers, New York, 1987.

[4] Saad, S. A.; Isa, K. Md.; Bahari, R. Chemically modified sugarcane bagasse as a potentially low-cost biosorbent for dye removal. Desalination, 2010, 264, 123-128.

[5] Sajab, M. S.; Chia, C. H.; Zakaria, S.; Jani, S. M.; Ayob, M. K.; Chee, K. L.; Khiew, P. S.; Chiu, W. S. Citric acid modified kenaf core fibers for removal of methylene blue from aqueous solution, Bioresour. Technol., 2011, 102, 7237-7243.

[6] Ma, J.; Yu, F.; Zhou, L.; Jin, L.; Yang, M.; Luan, J.; Tang, Y.; Fan, H.; Yuan, ZEnhanced adsorptive removal of methyl orange and methylene blue from aqueous solution by alkali-activated multiwalled carbon nanotubes. J. Appl. Mater. Interfaces, 2012, 4(11), 5749-5760.

[7] H.J. Kim, W.I. Kim, T.J. Park. To complet it Highly dispersed platinum carbon aerogel catalyst for polymer electrolyte membrane fuel cells. Carbon, 2008, 46, 1393-1400.

[8] Deegan, A.M; Shaik, B.; Nolan, K. , Treatment options for wastewater effluents from pharmaceutical companies, Int. J. Environ. Sci. Technol. 2011, 8, 649-666.

[9] Mezohegvi, G.; van der Zee, F. P. Towards advanced aqueous dye removal processes: a short review on the versatile role of activated carbon. J. Environ. Manage. 2012, 102, 148-164

[10] Oliveira, L. C. A.; Rios, R. V. R. A. Activated carbon/iron oxide magnetic composites for the adsorption of contaminants in water, Carbon, 2002, 40, 2177-2183.

[11] Clifford, D.; Chu, P.; Lau, A. Thermal regeneration of powdered activated carbon (PAC) and PAC biological sludge mixtures, Water Res. 1983, 17, 1125-1138.

[12] Shieh, F. K.; Hsiao, C. T.; Kao, H. M.; Sue, Y. C.; Lin, K. W.; Wu, C. C.; Chen, X. H.; Wan, L.; Hsu, M. H.; Hwu, J. R.; Tsung, C. K., Wu, K. C. W. Size-adjustable annular ring-functionalized mesoporous silica as effective and selective adsorbents for heavy metal ions. RSC Adv., 2013, 3(48), 25686-25689.

[13] Wu, H. Y.; Shieh, F. K.; Kao, H. M.; Chen, Y. W., Deka, J. R.; Liao, S. H.; Wu, K. C. W. Synthesis, Bifunctionalization, and Remarkable Adsorption Performance of Benzene-Bridged Periodic Mesoporous Organosilicas Functionalized with High Loadings of Carboxylic Acids. Chemistry-A European Journal. 2013, 19(20), 6358-6367.

[14] Whittaker, P. B.; Wang, X.; Zimmermann, W.; Lieb, K. R.; Chua, H. T. Predicting the Integral Heat of Adsorption for Gas Physisorption on Microporous and Mesoporous Adsorbents. J. Phys. Chem. C, 2014, 118 (16), 8350–8358.

[15] Hristov, J.; Fachikov, L. An overview of separation by magnetically stabilized beds: sate of the art and potential applications. China Particuology, 2007, 5, 11-18.

[16] Marel, H.W.v.d.; Beutelspacher, H. Atlas of Infrared Spectroscopy of Clay Minerals and their Admixtures, Elsevier, Amsterdam, 1976.

[17] Darezereshki, E.; Bakhtiar, F.; Vakylabad, A. B.; Hassani Z. Single-step synthesis of activated carbon/ γ- Fe_2O_3 nano composite at room temperature. Materials Sc. in Semiconductor Processing, 2013, 16, 221-225.

[18] Ranjithkumar, V.; Sangeetha, S.; Vairam, S. Synthesis of magnetic activated carbon/γ-Fe_2O_3 nano composite and its application in the removal of acid yellow 17 dye from water. J Hazard. Mater. 2014, 273, 127-135.

[19] Jiles, D. Introduction to Magnetism and Magnetic Materials, Chapman and Hall, 1991.

[20] Kyzas, G. Z.; Kostoglou, M.; Lazaridis, N. K. Relating interaction of dye molecules with chitosan to adsorption kinetic data. Lagmuir, 2010, 26(12), 9617-9626.

[21] Ahmaruzzaman, M.; Reza, R.A. Decontamination of cationic and anionic dyes in single and binary mode from aqueous phase by mesoporus pulp waste. Environ. Progress. Sustain. Energy 2014, In press.

[22] Qada, E.N. E.; Allen, S.J.; Walker, G.M. Adsorption of basic dyes from aqueous solution onto activated carbons. Chem. Eng. J. 2008, 135, 174–184.

[23] Janaki, V.; Vijayaraghvan, K.; Ramasamy, A.K.; Lee, K. J.; Oh, B. T.; Kamala-Kannan, S. Competitive adsorption of reactive orange 16 and Reactive Brilliant Blue R on plyaniline/bacterial extracellular polysaccharides composite- A novel eco-friendly polymer. J. Hazard. Mater. 2012, 241-242, 110-117.

[24] Nethaji, S.; Sivasamy, A.; Mandal, A. B. Preparation and characterization of corn cob activated carbon coated with nano-sized magnetite particles for the removal of Cr(VI). Bioresource Technology. 2013, 134, 94-100.

[25] Shao, L.; Ren, Z.; Zhang, G.; Chen, L. Facile synthesis, characterization of a MnFe2O2/activated carbon magnetic composite and its effectiveness in tetracycline removal. Material Chemistry and Physics, 2012, 135, 16-24.

[26] Batzias, F.A.; Sidiras, D.K. Simulation of dye adsorption by beech sawdust as affected by pH, J. Hazard. Mater. 2007, 141, 668-679.

[27] Reza, R. A.; Ahmaruzzaman, M.;.Sil, A. K; Gupta, V.K. Comparative adsorption behaviour of clofibric acid and Ibuprofen onto microwave assisted activated bamboo waste, Ind. Eng. Chem. Res 2014, 53, 9331-9339.

[28] Ahmaruzzaman, M.; Reza, R .A.; Ahmed, Md. J.K.; Sil, A. K. Scavenging behaviour of Schumannianthus dichotomus-Derived activated carbon for the removal of methylene blue from aqueous phase, Environ. Progress. Sustain. Energy 2014, 33, 1148-1157.

[29] Reza, R.A.; Ahmaruzzaman, M. Comparative study of waste derived adsorbents for sequestering methylne blue form aquatic environment, J. Environ. Chem. Eng. (2014) .doi.org/10.1016/j.jece.2014.06.006

[30] Reza, R. A.; Ahmed, Md. J.K.; Sil, A. K.; Ahmaruzzaman, M. A non-conventional adsorbent for the removal of clofibric acid from aqueous pahse. 2014, 49, 1592-1603.

[31] Travlou, N.A.; Kyzas, G.Z.; Lazaridis, N.K.; Deliyanni, E.A. Graphene oxide/chitosan composite for reactive dye removal. Chem. Eng. J. 2013, 217, 256-265.

[32] Travlou, N. A.; Kyzas, G. Z.; Lazaridis, N. K.; Deliyanni E. A.; Fictionalization of grapheme oxide with magnetic chitosan for the preparation of nano composite dye adsorbent. Langmuir, (2013), 29, 1657-1668.

[33] Guo, Y.; Du, E. The Effect of thermal regeneration conditions and inorganic compounds on the characteristics of activated carbon used in power plant. Energy Proc. 17 (Part A), 2012, 444-449.

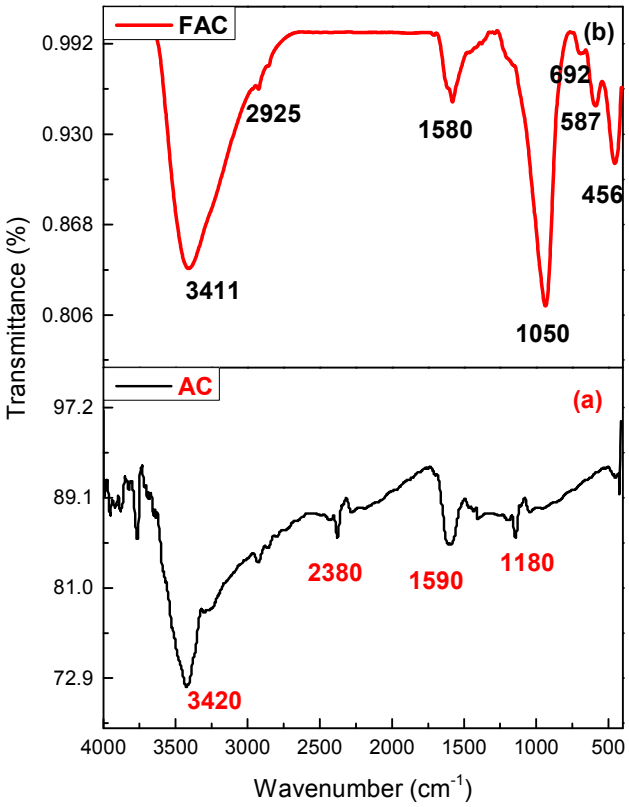

Fig.1 FTIR spectra of (a) AC and (b) FAC

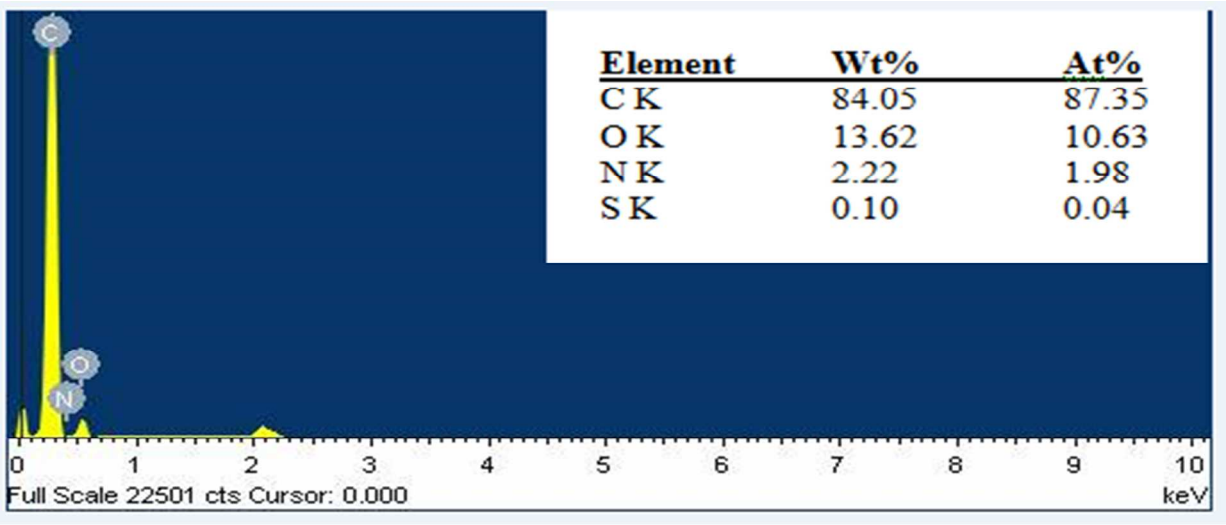

Fig. 2(a) EDS spectra of AC

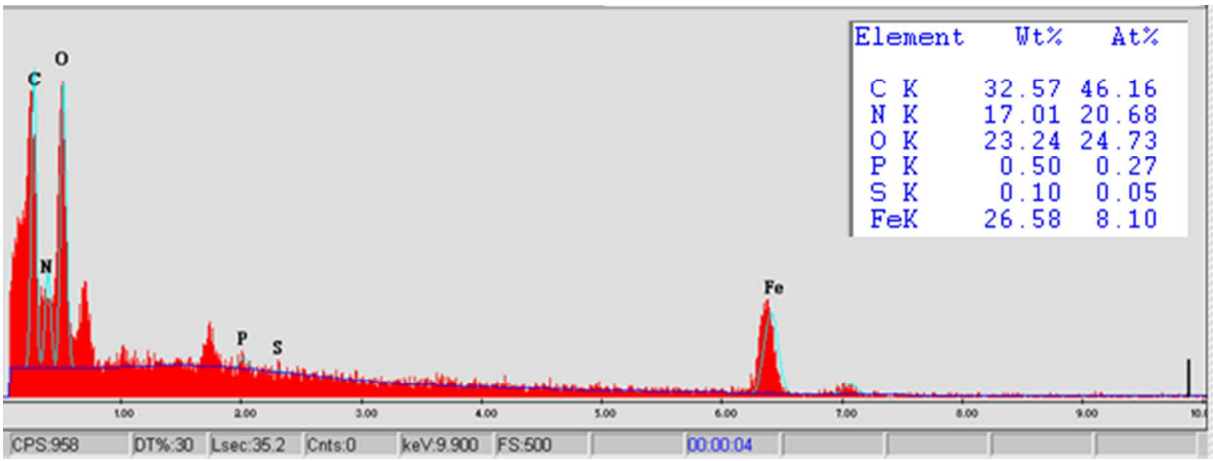

Fig. 2 (b) EDS spectra of FAC

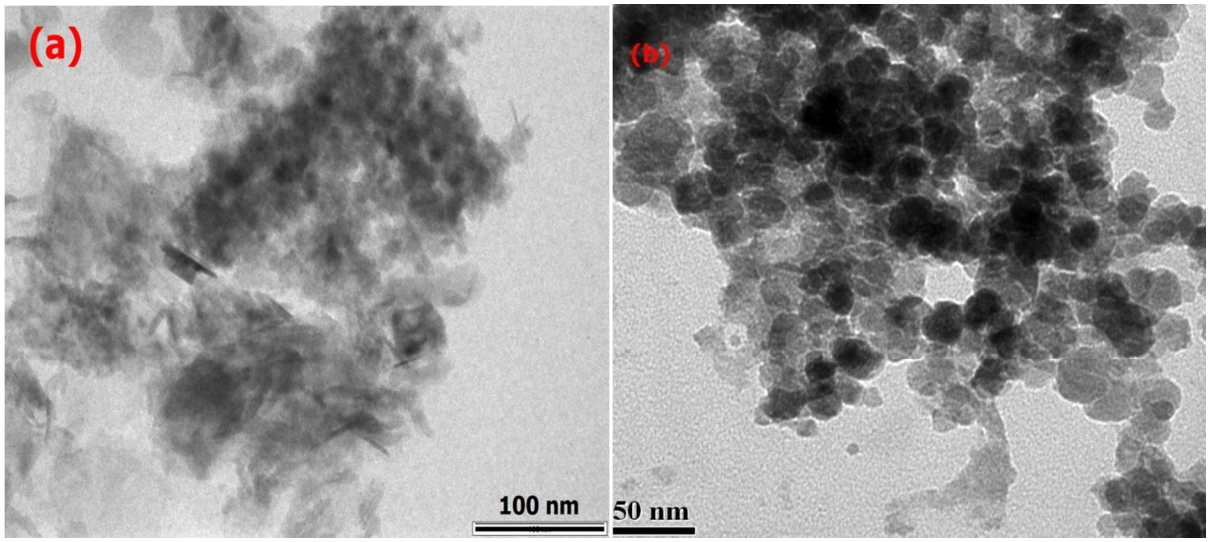

Fig. 3(a) TEM image of AC (b) TEM image of Fe_2O_3

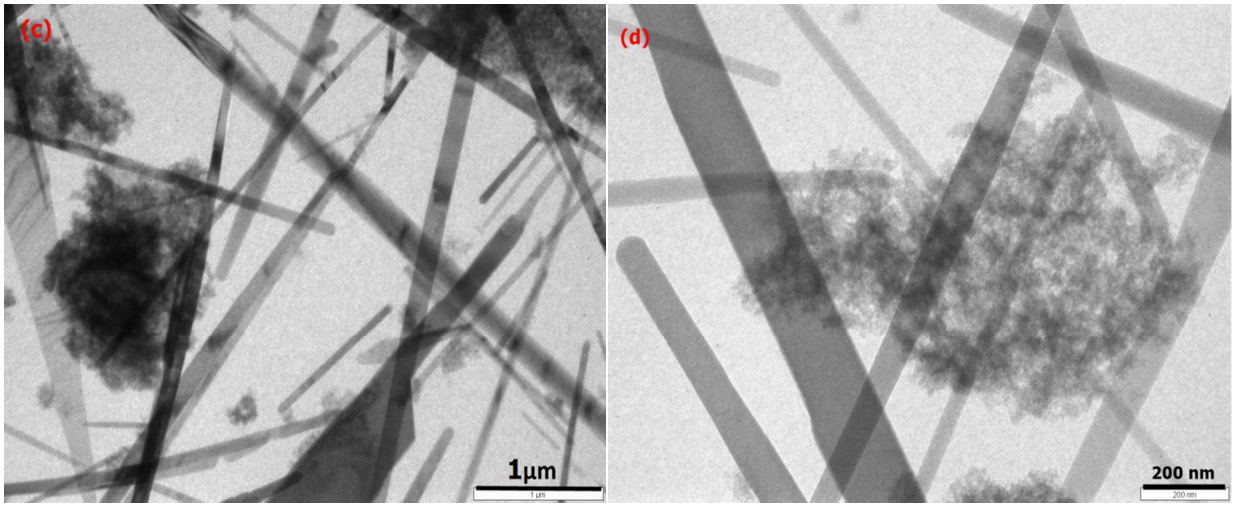

(c) TEM image of FAC (Low Magnification) (d) TEM image of FAC (High Magnification)

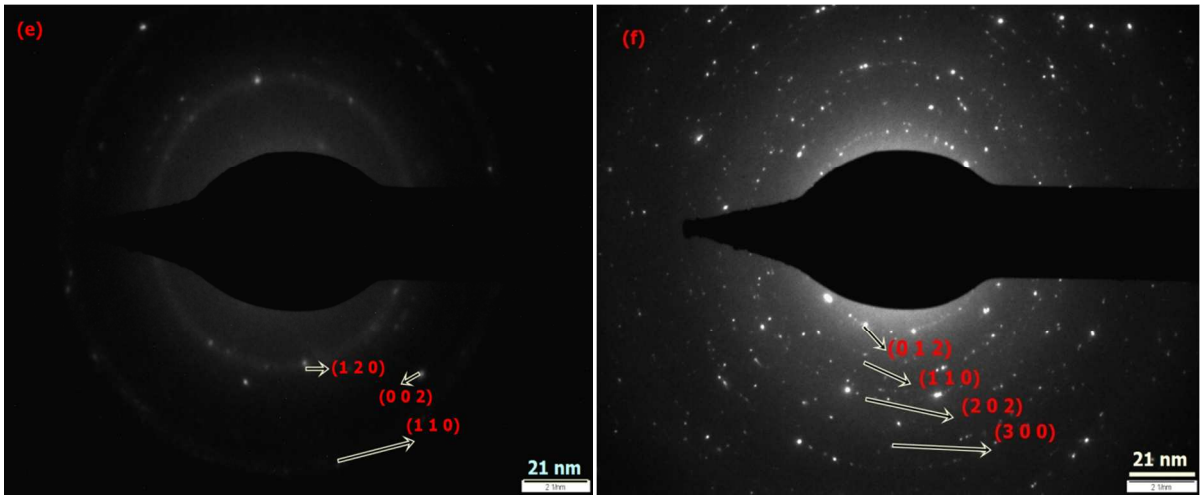

(e) SAED pattern of AC

(f) SAED pattern FAC

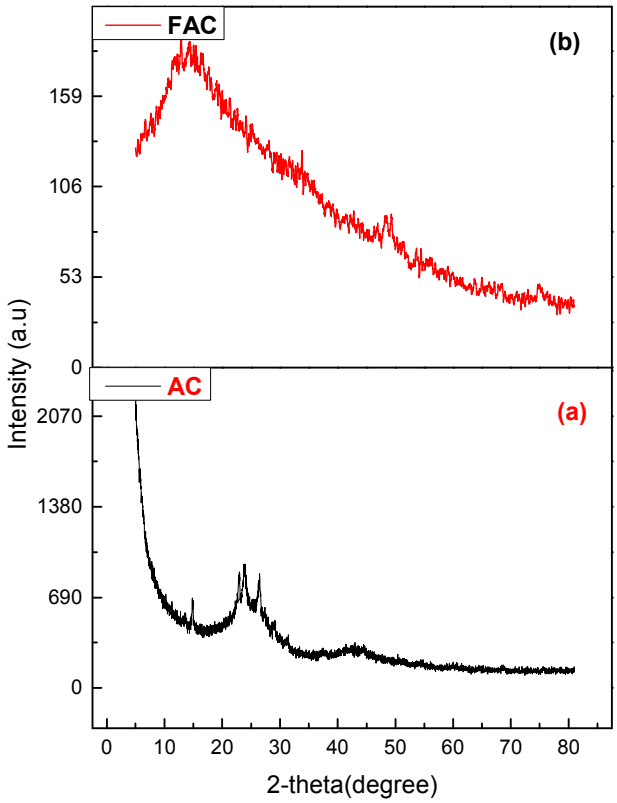

Fig.4 P-XRD of AC and FAC

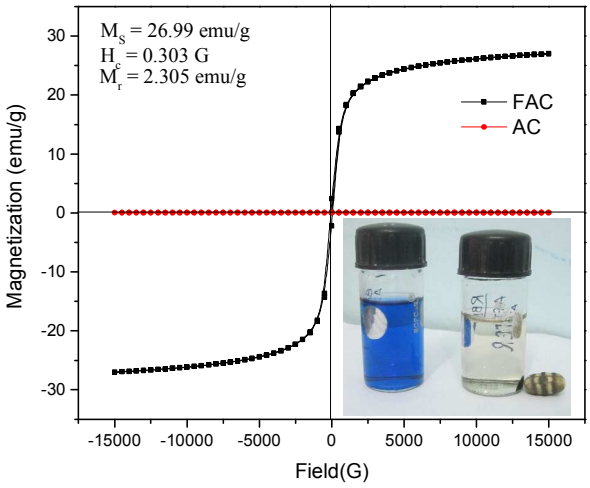

Fig. 5 Magnetization curves of FAC

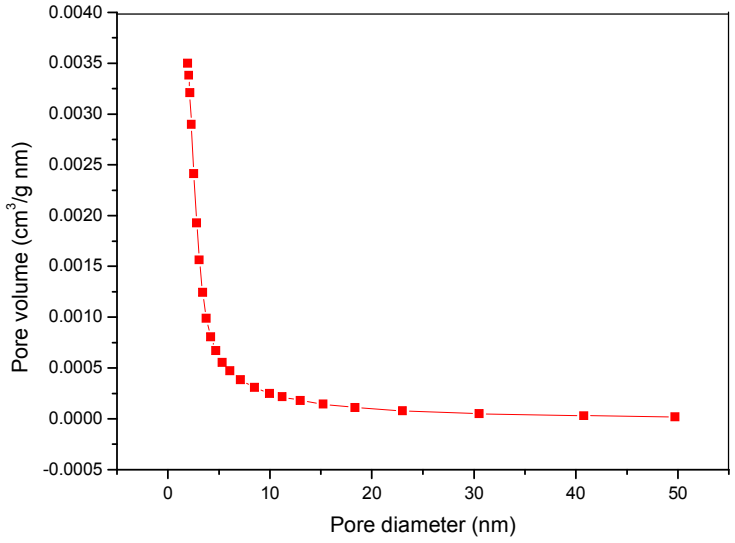

Fig.6 Pore distribution of FAC

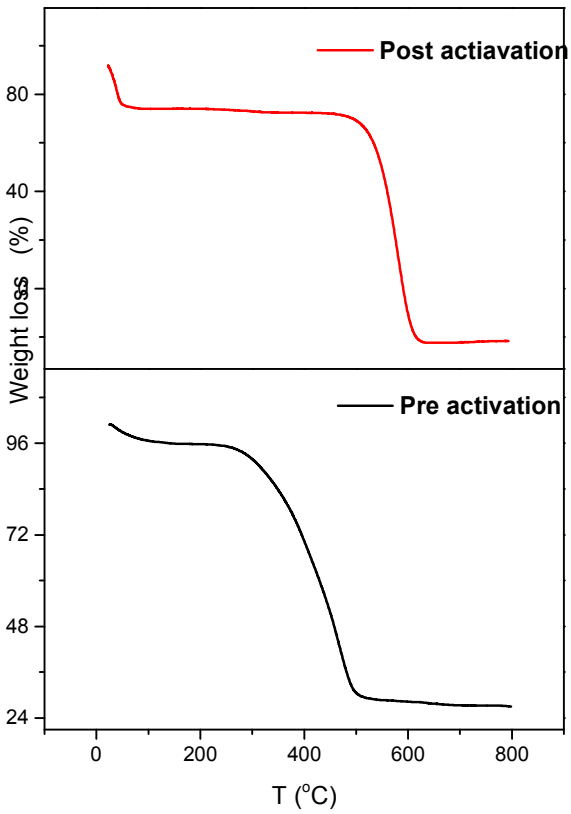

Fig. 7 TGA curve of AC before and after activation

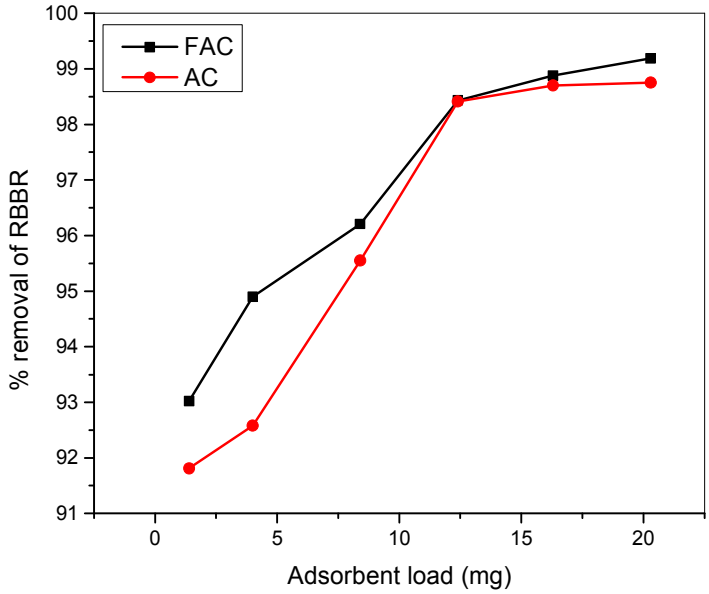

Fig. 8 Comparison of % removal of RBBR onto AC and FAC

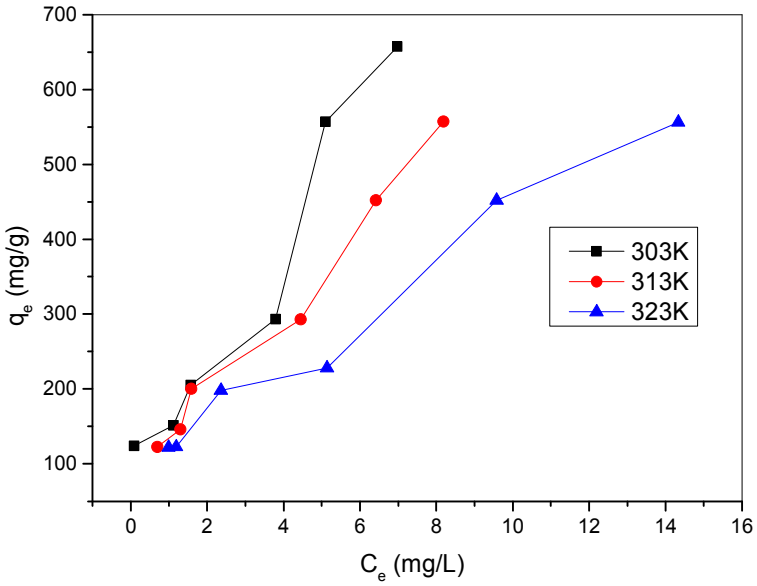

Fig. 9 Impact of temperature on adsorption capacity of RBBR

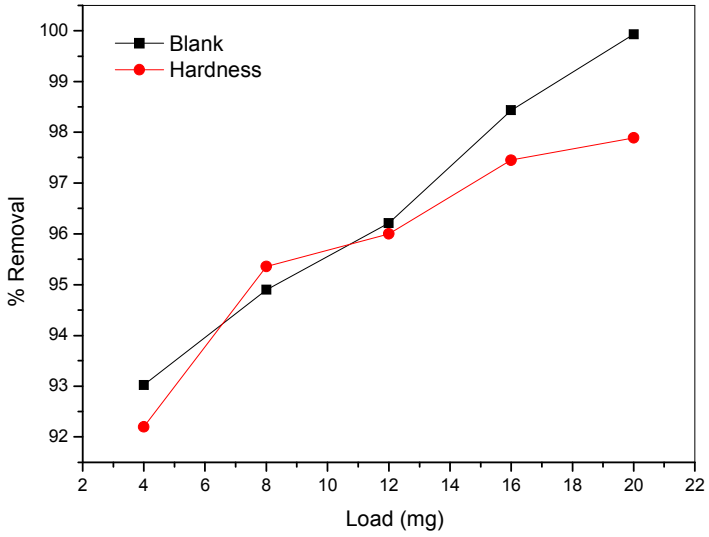

Fig.10 Influence of hardness in the retention of RBBR

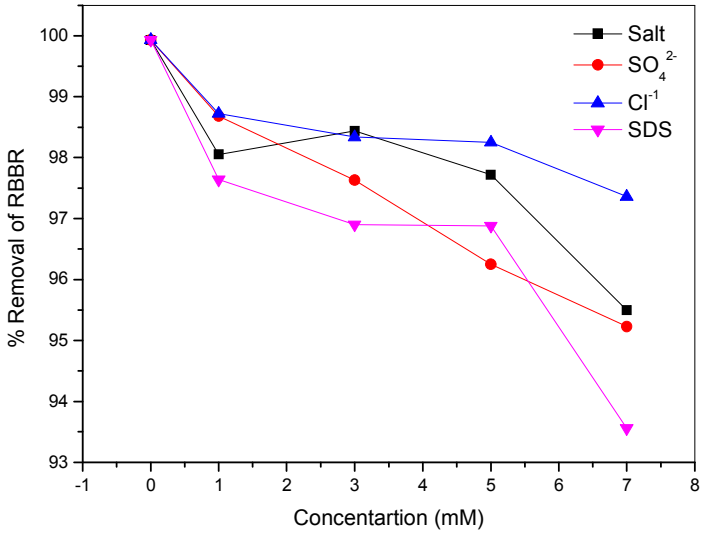

Fig. 11 Impact of ionic strength in the removal of RBBR

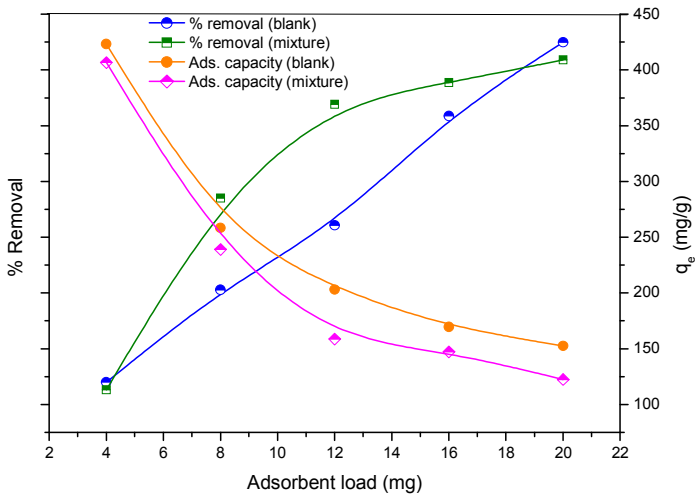

Fig.12 Impact of simulated mixture on the removal RBBR

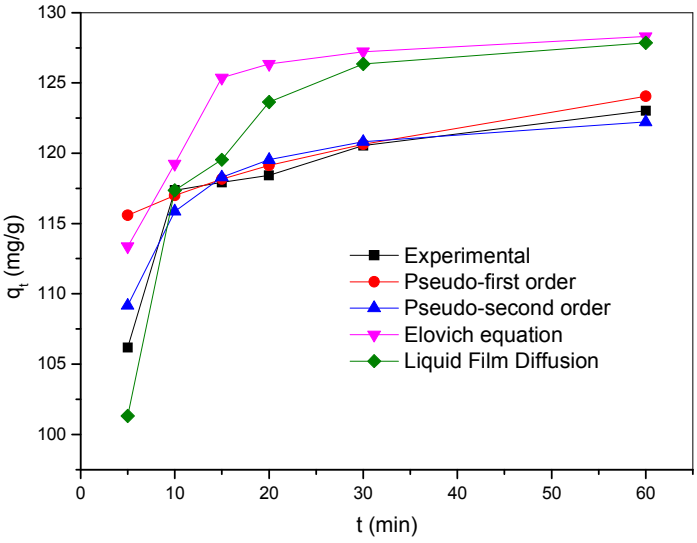

Fig.13 Validity of kinetic models with experimental data at 303K

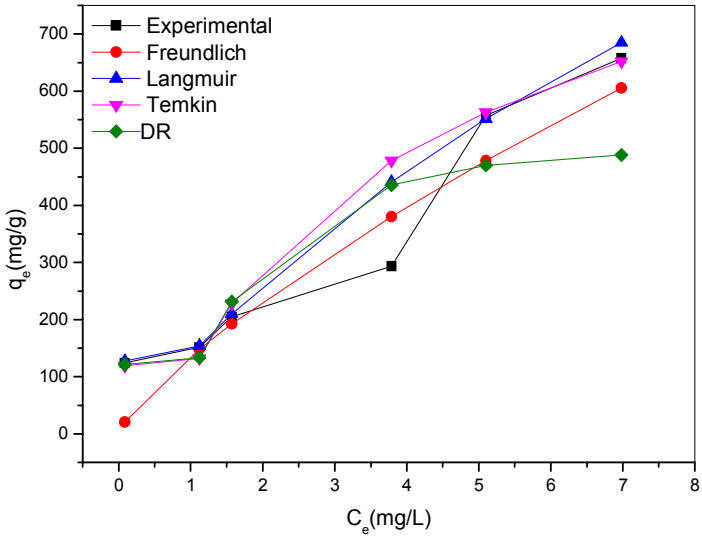

Fig.14 Validity of adsorption isotherm with experimental data at 303K

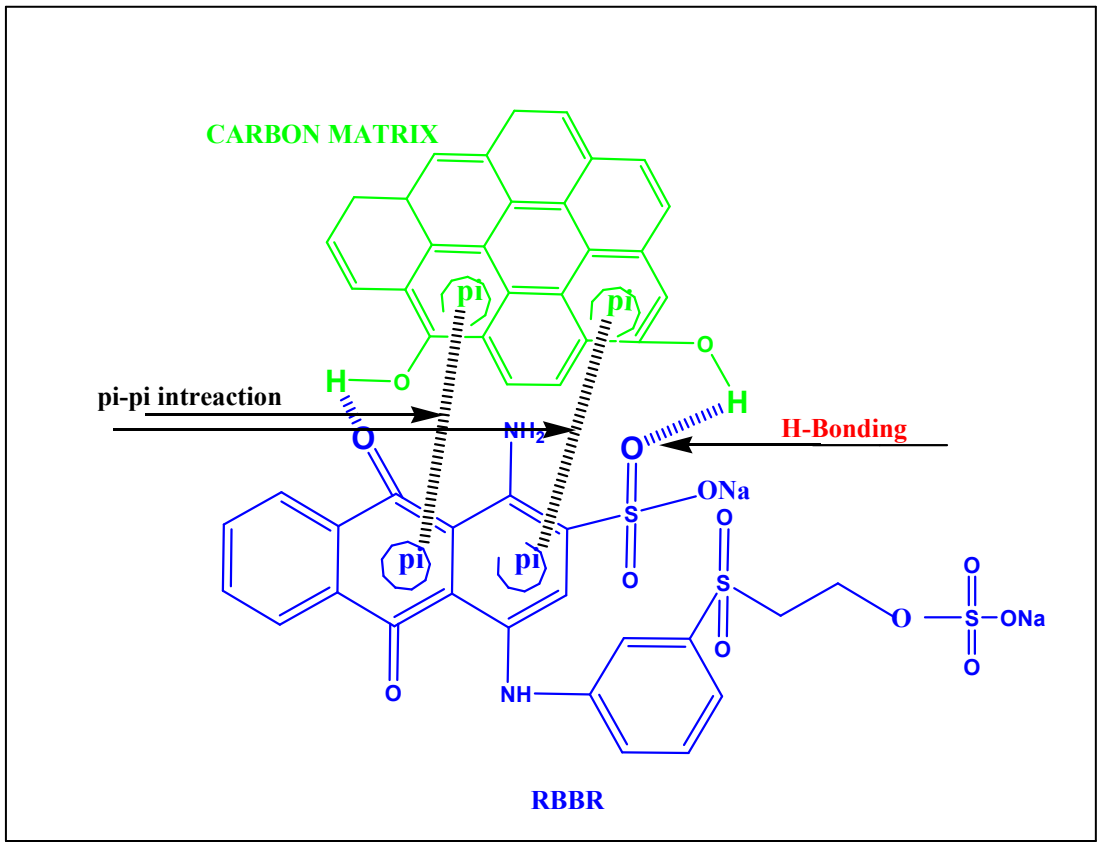

Fig. 15 Proposed mechanisms for RBBR adsorption onto FAC

Table 1. Kinetic models parameters for adsorption of RBBR onto FAC

Kinetic model	Model parameters	Values
Pseudo- first order	$q_{e,\,exp}$ (mg.g^{-1})	124.12
	$q_{e,\,cal}$(mg.g^{-1})	10.19
	k_1(g.mg^{-1}. min^{-1})	0.0359
	R^2	0.9532
	$\Delta q\%$	16.85
Pseudo-second order	$q_{e,\,cal}$(mg.g^{-1})	123.45
	k_2 (g.mg.min^{-1})	0.0123
	R^2	0.9998
	$\Delta q\%$	0.241
Elovich equation	a (mg g^{-1} min$^{-0.5}$)	1.02×10^{19}
	b	0.3841
	R^2	0.8301
Liquid film diffusion	k_{fd} (min^{-1})	2.49
	I_{fd}	0.0358
	R^2	0.9521

Table 2(a). Langmuir Isotherm parameters and their respective error functions for adsorption of RBBR onto FAC

T (K)	a_L $mg.g^{-1}$	b_L $L.g^{-1}$	R_L	R^2	Sum of the Square of the errors (ERRSQ)	Hybrid fractional error (HYBRID)	Marquardt's percent standard deviation (MPSD)	Average relative error (ARE)	Sum of absolute error (EABS)
303		211.05	0.70	0.9803	22642.3	1893.63	13.67	10.44	189.32
313		107.20	1.31	0.9513	11173.13	1058.76	9.35	9.26	199.75
323		76.92	1.62	0.9871	15994.49	1761.21	16.14	13.63	188.28

Table 2(b). Freundlich Isotherm parameters and their respective error functions for adsorption of RBBR onto FAC

T (K)	$1/n_F$	b_L $mg.g^{-1}$	R^2	Sum of the Square of the errors (ERRSQ)	Hybrid fractional error (HYBRID)	Marquardt's percent standard deviation (MPSD)	Average relative error (ARE)	Sum of absolute error (EABS)
303	0.77	134.89	0.9339	27401.01	3211.36	40.98	23.89	337.25
313	0.60	138.03	0.9635	7290.85	488.06	87.26	30.50	177.24
323	0.45	120.22	0.9205	35632.76	1824.38	8.15	13.61	317.37

Table 2(c). Temkin Isotherm parameters and their respective error functions for adsorption of RBBR onto FAC

T (K)	B	$\frac{K_{Tem}}{L.g^{-1}}$	R^2	Sum of the Square of the errors (ERRSQ)	Hybrid fractional error (HYBRID)	Marquardt's percent standard deviation (MPSD)	Average relative error (ARE)	Sum of absolute error (EABS)
303	238.84	1.42	0.9950	35152.34	3044.30	4.07	15.49	243.14
313	208.74	1.57	0.9872	14538.19	1194.13	6.16	9.71	182.35
323	164.48	1.78	0.9815	20874.02	2269.33	20.10	15.28	218.99

Table 2(d). Dubunin-Radushkevich Isotherm parameters and their respective error functions for adsorption of RBBR onto FAC

T (K)	Ψ_D	ϕ_D	R^2	Sum of the Square of the errors (ERRSQ)	Hybrid fractional error (HYBRID)	Marquardt's percent standard deviation (MPSD)	Average relative error (ARE)	Sum of absolute error (EABS)
303	3.36	523.21	0.8168	57679.64	3297.82	17.83	19.48	446.39
313	2.29	468.71	0.8721	52437.43	4995.08	45.48	35.53	547.90
323	34.48	572.49	0.8731	23066.85	2943.25	19.72	20.20	353.85